Periodicity manifestations in the turbulent regime of the globally coupled map lattice

Tokuzo Shimada and Kengo Kikuchi
Department of Physics, Meiji University, Higashi-Mita 1-1-1, Kawasaki, Kanagawa 214-8571, Japan
(Received 15 April 1998; revised manuscript received 3 April 2000)

We revisit the globally coupled map lattice. We show that in the so called turbulent regime various periodic cluster attractor states are formed, even though the coupling between the maps are very small relative to the nonlinearity in the element maps. Most outstanding is a maximally symmetric three cluster attractor in period-3 motion, due to the foliation of the period-3 window of the element logistic maps. An analytical approach is proposed which successfully explains the systematics of various periodicity manifestations in the turbulent regime. The linear stability of the period-3 cluster attractors is investigated.

PACS number(s): 05.45.−a, 05.90.+m, 87.10.+e

I. INTRODUCTION

Recently there has been much progress in the study of synchronization of nonlinear maps [1–7] and flows [8–12]. This may lead to a clarification of the intelligence activity supposed to come from the synchronization among the neurons in the neural network. In particular, the globally coupled map lattice (GCML) may be considered one of the basic models for network systems, expressing their characteristic limits. In its simplest form, all elements interact among themselves via their mean fields, with a common coupling, and each of the elements is a simple logistic map with a given nonlinearity. This theory may be regarded as a natural extension of spin-glass theories [13,14] to the nonlinear dynamics. Even though the simplest GCML has only two model parameters—the common nonlinearity parameter a and the overall coupling ε—it exhibits a rich variety of interesting phases in the parameter space corresponding to various forms of synchronization among the maps determined by the balance between the randomness specified by a and the coherence by ε.

In this paper we revisit the turbulent regime of the GCML, which is a regime in parameter space with high a and very small ε. The main interest in this regime has so far focused to so called hidden coherence [2,3]. In this phenomenon the fluctuation of the mean field of the maps in the evolution does not cease at a large system size. The mean field distribution obeys the central limit theorem (CLT), but not the law of large numbers (LLN) [2,4]. We show that the dynamics of the GCML in this regime is a foliation of that of the element logistic maps, and that various periodic cluster attractors are formed, even though the coupling between the maps is set very small. We show that regions which may be described by the hidden coherence do exist, but that they comprise a very limited part of the parameter space.

We organize our discussion into three parts. First we present results of an extensive phenomenological survey of this regime, and list evidence of periodicity manifestations due to the periodic windows of the element logistic map. Most outstanding is the onset of period-3 cluster attractors. The turbulent regime is, if we may say, a bizarre region with many faces—drastic periodicity manifestations as well as almost perfect randomness under the hidden coherence. At periodic or quasiperiodic attractors, the mean field evolves, controlled by the scale of the cluster orbits, and the LLN is naturally violated. We also present remarkable data which show that a GCML at a large system size acquires a high sensitivity to the periodic windows of the element map. Second, we present an analytical approach which successfully explains the systematics of the periodicity manifestations. We present a tuning condition which limits the system parameters with which GCML cluster attractor states of a given periodicity may be formed. The key to obtaining the condition is the introduction of the maximally symmetric cluster attractor (MSCA), which is a solution of minimum fluctuation in the mean field. This corresponds to the known state of two clusters in an opposite phase oscillation which is formed in the ordered phase of the GCML [1]. We verify the validity of the condition in detail, and show that the foliation is the governing dynamics of this regime.

Third, we show that the period-3 cluster attractors formed in the turbulent regime are linearly stable, and investigate how their stability changes by the coupling ε and the population ratios. In particular, we algebraically derive the ε value for the formation of the most linearly stable bifurcated MSCA (MSCA*).

The organization of this paper is as follows. In Sec. II we briefly review various GCML phases, and locate the turbulent regime in the parameter space. We then summarize the known facts of this regime. No originality is claimed here. We then briefly compare them with our results. In Sec. III we present our phenomenological findings, including the period-3 MSCA and an associated fewer cluster attractor. In Sec. IV we present an analytical approach which explains successfully how the periodic windows of the element map control the GCML dynamics in the turbulent regime. In Sec. V we investigate the stability of the cluster attractors. We conclude in Sec. VI.

II. GCML PHASE STRUCTURE AND THE TURBULENT REGIME: A REVIEW

In this paper we study the simplest GCML, which is a system of N maps evolving by

$$x_i(n+1)=(1-\varepsilon)f(x_i(n))+\varepsilon h(n), \quad (i=1,\ldots,N), \tag{2.1}$$

and the mean field $h(n)$ of maps is defined as

$$h(n) \equiv \frac{1}{N} \sum_{i=1}^{N} f(x_i(n)) = \frac{1}{N} \sum_{i=1}^{N} x_i(n+1). \qquad (2.2)$$

In the first step, all x_i's are simultaneously mapped by a nonlinear function f. The function f could be distinct maps (heterogeneous GCML's), but in this paper we consider the simplest case that f is a logistic map $f(x)=1-ax^2$ common to all variables (homogeneous GCML's). The nonlinearity of f generally magnifies the variance among the maps. The larger the parameter a is, the more strongly the variance is enhanced. In the second step, the maps undergo interaction between themselves, with a global coupling constant ε. Here each $f(x_i)$ is pulled to the mean field $h(n)$ at a fixed rate $1-\varepsilon$. The larger the coupling ε is, the more strongly the maps are driven into synchronization.

The model is endowed with various interesting phases under a subtle balance between the two conflicting tendencies. The phase diagram in the a,ε plane was explored by Kaneko [1]. Let us explain the phases, choosing $a=1.80$ for definiteness. This is far above the criticality $a=1.401\ldots$ to the chaos for a single logistic map. (i) For a sufficiently large ε ($\gtrsim 0.38$) the maps are strongly bunched together in a cluster in the final attractor, and evolve chaotically as a single logistic map. This is the *coherent phase*. (ii) For $\varepsilon=0.22$–0.30, the interaction via the mean field no longer exerts a strong bunching, and the final maps divide into two clusters. The maps in each cluster are still tightly synchronized with each other, and the two clusters mutually oscillate oppositely in phase. This phase turns out to be a solution of a minimum fluctuation in the mean field, and is called a *two-clustered ordered phase*. (iii) For smaller ε, the number of final clusters increases, but it remains independent of the total number of maps in the system. The typical number of clusters at various ε ranges is indicated in the phase diagram [1]. (iv) Finally, for a very small ε the number of clusters is in general proportional to N. This region is called the *turbulent regime*. This is the target region of our analysis.

It is known that in the turbulent regime maps evolve almost randomly at a small lattice size N, and that there occurs a subtle correlation—a hidden coherence—at large N. But, as we show below, there actually emerge drastic global periodic motions of maps if the ε's takes certain values for a given a. Let us first briefly review previous observations in the literature.

(i) The final state of the GCML in this regime iterated from a random configuration consists of maps and tiny clusters, each moving chaotically due to high nonlinearity. The number of elements (maps and clusters) is proportional to the number of whole maps, in sharp contrast to the ordered regime [2].

(ii) There emerges a certain coherence between elements when the size N is large [2,4]. If $x_i(n)$ $(i=1,\ldots,N)$ are really independent random variables following a common probability distribution, the mean squared deviation (MSD) of the mean field $h(n)$ ($\delta h^2=\langle h^2\rangle-\langle h\rangle^2$ with $\langle\cdots\rangle$ here meaning the long time average) should decrease proportionally to $1/N$ by the LLN, and the $h(n)$ distribution must be a Gaussian for sufficiently large N by the CLT. However, there is a certain threshold in N (depending on both a and ε) above which the MSD ceases to decrease even though the distribution remains Gaussian; the CLT holds but not the LLN [2]. This reflects some hidden coherence between the maps in evolution. In fact the LLN is restored when a tiny noise term is introduced in each map independently [3,4].

(iii) The violation of the LLN reflects that the map probability distribution $\rho(x)$ depends on time. Indeed, a noise intensity analysis of ensembles successfully proves the LLN [3]. If the LLN should hold in the time average, $\rho(x)$ would have to be a fixed point distribution of the Frobenius-Perron evolution equation [15]. It has been argued that the fixed point distribution may be unstable due to the periodic windows of the logistic map [4], though this point is controversial. For instance, on tent maps, the same instability occurs but no periodic windows are present [16]. The coherence manifests itself in mutual information [2]. On the other hand, a temporal correlation function similar to the Edwards-Anderson order parameter for the spin glass [14] decays to zero exponentially. Thus it may not be due to freezing between two elements [2].

The hidden coherence was found in a statistical analysis of the mean field fluctuation [2]. But there has been no report of an extensive statistical analysis which covers the whole turbulent regime as well as a wide range of the system size. Once we have done this, we are faced with a bizarre feature of the turbulent regime: the hidden coherence is one thing, but there also occur drastic global periodicity manifestations. The above lists are correct but need reservations.

For (i), there is a need for a careful reservation on the coupling values. We show below that, when the coupling ε takes small but tuned values for a given a, the maps again—as in the ordered phase—may split into a few bound clusters in periodic motion. The most striking manifestation of periodicity in this form is states of almost equally populated clusters mutually oscillating in the same period with the number of clusters. We call this type of periodicity manifestation, MSCA, and present the tuning condition for it below. We label such a cluster attractor by the periodicity and the number of the clusters. For instance, we call the outstanding period-3 symmetric cluster state the $p3c3$ MSCA. There also occurs a bifurcated $p3c3$ MSCA. The MSD of the $h(n)$ distribution is very small in the MSCA or its bifurcated state, because of the good population symmetry among the clusters. At slightly larger ε, we observe that the number of clusters decreases while the orbits are approximately retained. A cluster attractor of this type ($p>c$) leads to a large MSD, which is independent of N.

As for (ii), we show below not only the LLN but also the CLT is violated in almost all regions in the turbulent regime. We pin down the very limited regions in the turbulent regime where the CLT holds with a violated LLN; only there may the term ''hidden coherence'' be used.

As for (iii), the decay exponent of the temporal correlator of the mean field fluctuations gradually decreases with the deviation of the coupling from the tuned value. Accordingly, the $h(n)$ distribution successively changes its shape from the highest rank sharp δ peaks down to the MSD-enhanced Gaussian distribution—the hidden coherence. This indicates

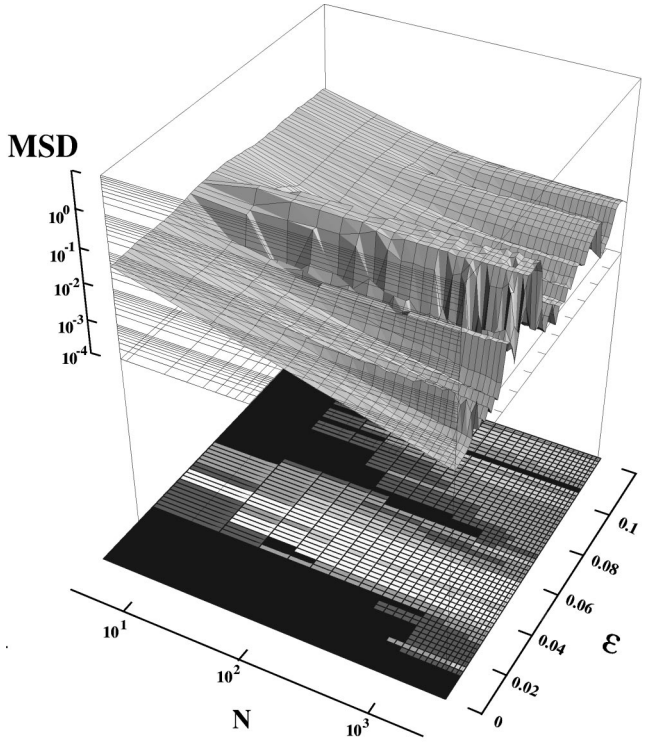

FIG. 1. The MSD surface of a mean field fluctuation (top), and the gray-scale density plot for the rank of distributions (bottom) on the $\varepsilon - N$ grid. $a = 1.90$, and the inclement $\Delta\varepsilon = 2 \times 10^{-3}$. The rank varies from zero (black) to 4 (white).

that the hidden coherence at the MSD valley may be the most modest periodicity remnant, being elusive due to high mixing.

The GCML can be defined in a one line equation, but its turbulent regime challenges us with so many faces ranging from a manifest periodicity to the hidden coherence. We consider that it is important to explore the systematics of periodicity manifestations by an extensive statistical survey, and present a sorted list of phenomenological observations. Below we first devote ourselves to this task.

III. PHENOMENOLOGY OF THE TURBULENT REGIME

A. Systematics in the mean field fluctuations

We start with an analysis of the distribution of the mean field fluctuation in time. In Fig. 1 we show its MSD at $a = 1.90$ as a surface over the $N - \varepsilon$ plane, which overlays a density plot of the periodicity rank of the $h(n)$ distribution. In order to set sufficiently fine grids for the surface, the system size is limited in the range $N < 4 \times 10^3$. For a wider range of N, in Fig. 2 we show the sections of the MSD surface at N in powers of ten up to 10^6.

1. Peak-valley structure of the MSD surface

First let us discuss the MSD surface and its sections. The linear edge of the surface at $\varepsilon = 0$ is of course due to the LLN. For a nonzero but very small ε ($\lesssim 0.01$), the LLN still holds to a good approximation but otherwise we can clearly see that the surface has many peaks along the N axis—the violation of the LLN in the time series.[1] There is a prominent peak at $\varepsilon \approx 0.040$–$0.050$—an extreme violation of the LLN—and in this ε range the MSD is in excess even for $N \approx 10^2$. In front of the peak there is a deep valley around $\varepsilon \approx 0.035$. We show below this peak and this valley are induced, respectively, by the $p3c2$ cluster attractor and the $p3c3$ MSCA (and its bifurcated state). Apart from these, the MSD surface systematically shows successive peak-valley structures at large N. We can see clearly in Fig. 2 how this structure is formed with an increase of N. At MSD peaks the LLN violation starts as early as $N = 10^2$–10^3, while in the valleys one has to wait until $N = 10^3$–10^4 in order to observe it. (In both cases, it starts to prevail from the larger ε side.) This twofold occurrence of the LLN violation leads to successive peak-valley structures around $N \approx 10^3$, which become outstanding at $N \approx 10^4$. Beyond that, up to the largest analyzed N ($= 10^6$), the MSD is independent of N, except for $\varepsilon \lesssim 0.005$, where the maps still approximately follow the LLN.

2. Mean field distributions

Now let us discuss the mean field distributions. In the rank density plot—the bottom panel of Fig. 1—the distribution is assigned a rank as follows.

(0) The distribution is Gaussian.[2] The MSD is the same within 20% error with that at $\varepsilon = 0$ with common a and N.

(1) Gaussian but with a sizably enhanced MSD (the hidden coherence). The MSD can be even factor of ten larger than the MSD by the LLN.

(2) A singly peaked distorted Gaussian, or a trapezoidal distribution.

(3) Either it has a few sharp peaks on top of a broad band, or it is an apparent overlapping Gaussian distribution. It manifestly shows the periodic motions of the maps.

(4) The distribution consists of a few sharp peaks only.

At rank 0 the $h(n)$ distribution obeys both the LLN and CLT, and the maps may be thought as independent random numbers with a common probability distribution. Conversely, at rank 4 the maps are in periodic motion, and so is the mean field. The ranks are organized in a way that the periodicity of the elements becomes more manifest with an increase of the rank. The MSD surface and the rank density plot both together reveal a simple rule: *The MSD is high wherever the rank is high, and vice versa. The rank distribution plot is almost a contour plot of the MSD surface*.[3]

---

[1]This does not imply the real violation of the LLN in the ensemble average [3]. The violation of the LLN means here that there is a larger fluctuation in the time series of $h(n)$ than expected by the LLN. We are interested in detecting the coherence among the evolving elements by the enhanced MSD.

[2]The $h(n)$ distribution cannot be a precise Gaussian, as it is limited in $[-x_L, x_L]$. When we discuss whether it is Gaussian or not, we are concerned whether the essence of the CLT, that the convolution of independent random distributions peaks like a Gaussian, is in action or not.

[3]The assignment of rank to each of thousands of distributions was a painful task. It was thrilling that two independently determined diagrams turned out to be a perfect match.

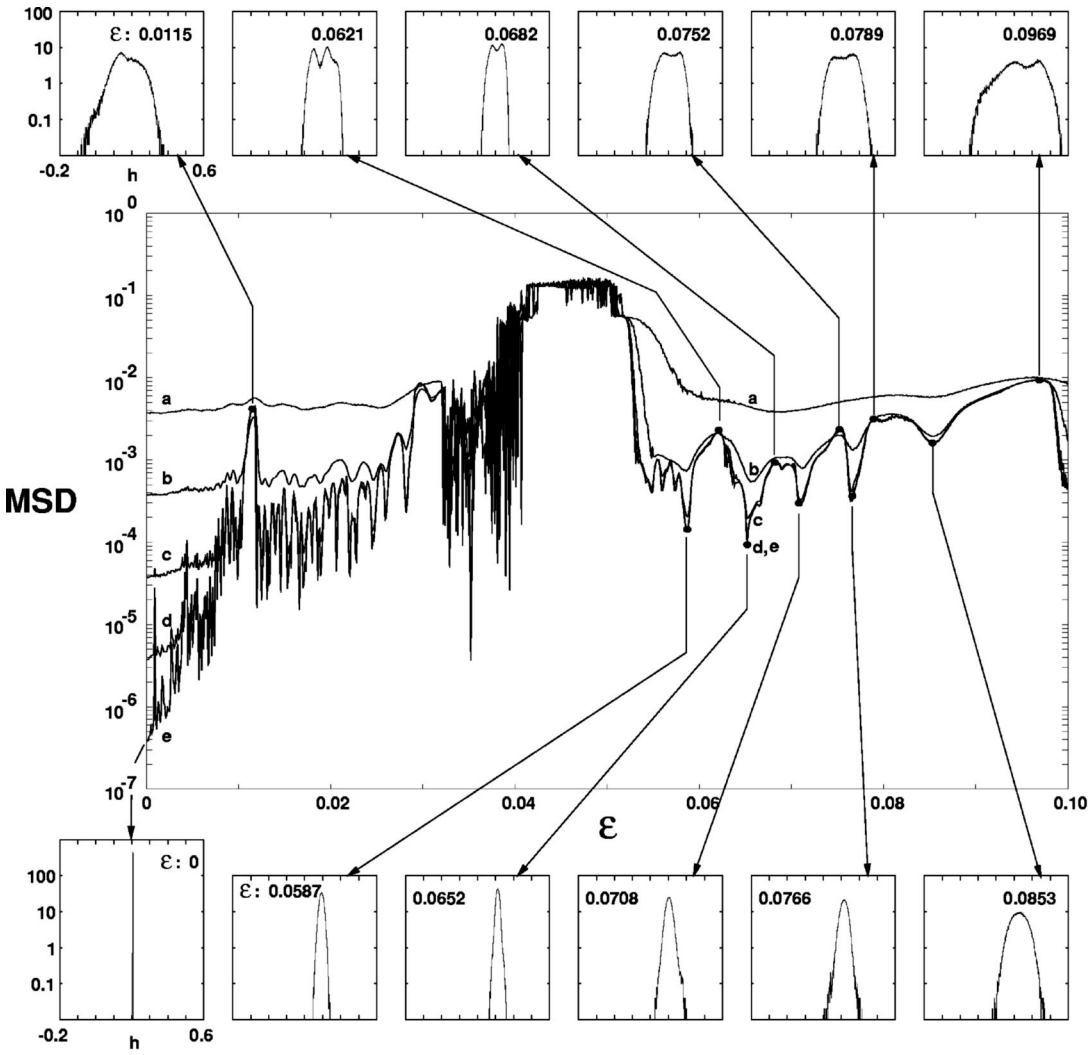

FIG. 2. Central diagram: the MSD at $a=1.90$ as a function of ε over $\varepsilon=0-0.10$ with inclement 10^{-4}. (a) $N=10^2$, (b) 10^3, (c) 10^4, (d) 10^5, and (e) 10^6. Top boxes: The $h(n)$ distributions at the MSD peaks. All are rank 3. Bottom: the same at valleys. All are rank 1 and correspond to the hidden coherence.

3. Regularity in the MSD enhancement

The above rule persists for larger N as well. In Fig. 2, for $N=10^6$ we show the $h(n)$ distributions at MSD peaks in the upper small boxes, and at valleys in the lower boxes. We find the following.[4]

(i) At any MSD peak, the rank is always high—rank 3. This tells us succinctly that the high MSD is induced by the maps evolving in a quasiperiodic motion at the peak ε values.

(ii) On the other hand, at any MSD valleys, the rank is 1 (the MSD-enhanced Gaussian), and reflects the hidden coherence.

In brief, *the MSD peaks at large N come from the quasiperiodic motion of the element maps, and the hidden coherence is restricted to the MSD valley at large N.*

We should add that the most prominent MSD peak and the deepest valley at the front of it are two extremes. At the former $(0.040<\varepsilon<0.050)$, the distribution is either rank 3 or even 4 and the MSD peak starts even at small N. The rank 4 distribution exhibits a periodic coherent motion of maps. We show below that this is due to the formation of a $p3c2$ cluster attractor; the lack of one cluster leads to a high MSD. At the latter, the distribution is also rank 4, but the MSD suppression is realized by the symmetrically populated $p3c3$ MSCA. We will briefly investigate the periodicity manifestation in general below, introducing other phenomenological means as well.

4. Hidden coherence revisited

The coherence, as observed by the violation of the LLN, occurs at any ε value in the range 0.005–0.12, except that the onset of the violation is earlier at MSD peaks (see Sec. III A 1). But the *hidden* coherence implies more: the MSD must be enhanced, but the mean field distribution must remain Gaussian—the rank must be 1.

[4]These two rules actually hold for $N=10^4$ up to the largest N $(=10^6)$ of our analysis. See below for a further discussion on the N dependence of the $h(n)$ distribution.

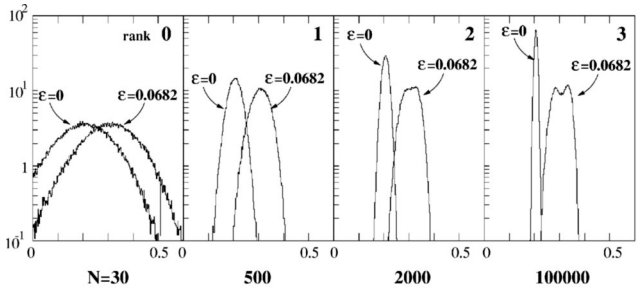

FIG. 3. The variation of the $h(n)$ distribution with a system size N at $a=1.90$, $\varepsilon=0.0682$, and $N=3\times10^1$, 5×10^2, 2×10^3, and 10^5 from left to right. Each is sampled in 10^5 iterations from a random start, discarding the first 10^4 steps, and compared with a reference distribution (rank 0). The rank is given on top.

To pin down the regions of the hidden coherence on the ε-N plane, let us investigate the change of the $h(n)$ distribution with the increase of N. Figure 3 exhibits a typical case, $\varepsilon=0.0682$, corresponding to one of the MSD peaks at $a=1.90$. Just when the LLN violation starts at $N=10^2$–10^3, the rank becomes 1. However, notably, for N beyond 10^3, the rank soon becomes 2 and simultaneously the MSD peak-valley structure appears. For $N\gtrsim10^4$, the rank becomes 3, and the peak-valley structure becomes remarkable. The regions of hidden coherence are thus restricted to a very small part. Excepting the transitive region $N\approx10^2$–10^3, only MSD valleys for the $h(n)$ distribution to remain Gaussian, and further, only in $N\gtrsim10^4$ for the MSD is enhancement. (The deepest MSD valley must be also excepted, since we observe the apparent periodic motion of $p3c3$ MSCA.)

B. The periodicity manifestation in the turbulent regime

The MSD peak-valley structure reflects a periodicity manifestation in the turbulent regime at various strengths depending on the value of ε. Let us substantiate this issue by the following quantities: (i) the distribution of maps and their mean field, (ii) map orbits, (iii) the temporal correlator of maps,[5] and (iv) the return map of $h(n)$. In Fig. 4, a is set at 1.90, and the above quantities are listed in a row for each typical iteration at a characteristic ε. The lattice size is fixed at $N=10^3$ in order to shed more light on the predominant period-3 window than the other windows.

1. p3c3 MSCA: the event at ε=0.036

Let us first investigate the region of the deepest MSD valley. In the map orbits we clearly find three lines showing the period-3 motion of maps in three clusters, and the map distribution shows three δ peaks. The mean field (the black circle) is almost constant due to the high population symmetry, and accordingly the $h(n)$ return map shows three almost degenerate points. The temporal correlator oscillates in period 3. All exhibit the formation of the $p3c3$ MSCA.

There is a slight subtlety in that the state is actually bifurcated—six clusters of maps with almost equal populations in the bifurcated period-3 motion. This is seen by the tiny split in the orbits near zero.[6] For $a=1.90$, the bifurcated $p3c3$ MSCA is always formed at $\varepsilon\approx0.035$, while at slightly higher ε (≈0.037–0.041) the final state is either a genuine $p3c3$ MSCA (90%) or an unstable period-3 cluster with high rate mixing (10%) depending on the initial configurations. We will come back to this point in Sec. V below.

2. p3c2 cluster attractor state: the event at ε=0.042

At the nearby stronger coupling ($\varepsilon\approx0.041$–0.051), the maps almost always split into two clusters with a population ratio of approximately 2:1, and the two clusters oscillate mutually in period 3. The map orbits sampled at $\varepsilon=0.042$ clearly exhibit this $p3c2$ state. The mean field oscillates in period 3 with a large amplitude due to the lack of one of the MSCA's, and hence leads to a prominent MSD enhancement. [Also see the three largely separated points in the $h(n)$ return plot, as well as the temporal correlator in period-3 motion.] Note that this high MSD is independent of the number of maps N—a way of violating the LLN—simply because the large N GCML dynamics is reduced to that of two clusters. The MSD is solely determined by the scale given by the cluster orbits and the population *ratios*. As a check let us try an estimate of the MSD. For the population ratio $\theta_1:\theta_2$, it is given by

$$(\delta h)^2=(S/3)(\theta_1^2+\theta_2^2-1/3)-(2T/3)(\theta_1^2+\theta_2^2-\theta_1\theta_2),$$

$$\theta_1+\theta_2=1, \tag{3.1}$$

with $S=\Sigma x_k$ and $T=\Sigma x_k x_{k+1}$. Let us take as approximations $\theta_1:\theta_2=2:1$, and the orbit points x_k at the tangent bifurcation point.[7] Then we obtain $(\delta h)^2=2^5/(3^37)\approx0.169$, in good agreement with the observed value 0.16 ± 0.01.

3. Peripheral point to the p3c3 MSCA: two events at ε=0.032

Here we have to account for the first transient behavior of the maps. In event (A), the maps drop into a $p3c3$ cluster attractor after a long iteration (at $n\approx8\times10^4$), while in event (B) they remain in a few unstable clusters in mutual period-3 motion until the last. Event (A) is essentially the same with the $p3c3$ MSCA event. We should only note that the broad lower band in the $h(n)$ distribution is an artifact of the first transient motion of maps. In event (B), the clusters are unstable, and there is a mixing of maps between the clusters; hence we can see only three clouds in the $h(n)$ return map. But the mixing rate is not so high as we can see from a gradual exponential decay[8] of the correlator with $\tau\approx140$, which clearly shows *a damped oscillation in period 3*.

---

[5] $C(t)=\langle\tilde{\mathbf{x}}(n+t)\cdot\tilde{\mathbf{x}}(n)/|\tilde{\mathbf{x}}(n+t)||\tilde{\mathbf{x}}(n)|\rangle$, with the relative vector $\tilde{\mathbf{x}}(n)\equiv(x_1(n)-h_n,\ldots,x_N(n)-h_n)$. The average $\langle\cdots\rangle$ is taken over n for the last 1000 steps.

[6] The six orbit points consist of three doublets of points, and the two points in a doublet are very close each other. We have checked this numerically, but the map distribution with the bin size 5×10^{-3} shows only three δ peaks.

[7] $a=7/4$ and $x_k=2/21+8/(3\sqrt{7})\cos[(\theta+2k\pi)/3]$, $k=0,1,2$, with $\theta=\tan^{-1}(3\sqrt{3})$ for the stable set. Numerically, (0.9983, −0.7440, 0.03140).

[8] We use τ, the number of steps in which the correlator decreases to 10^{-3}, as an estimate of the mixing rate.

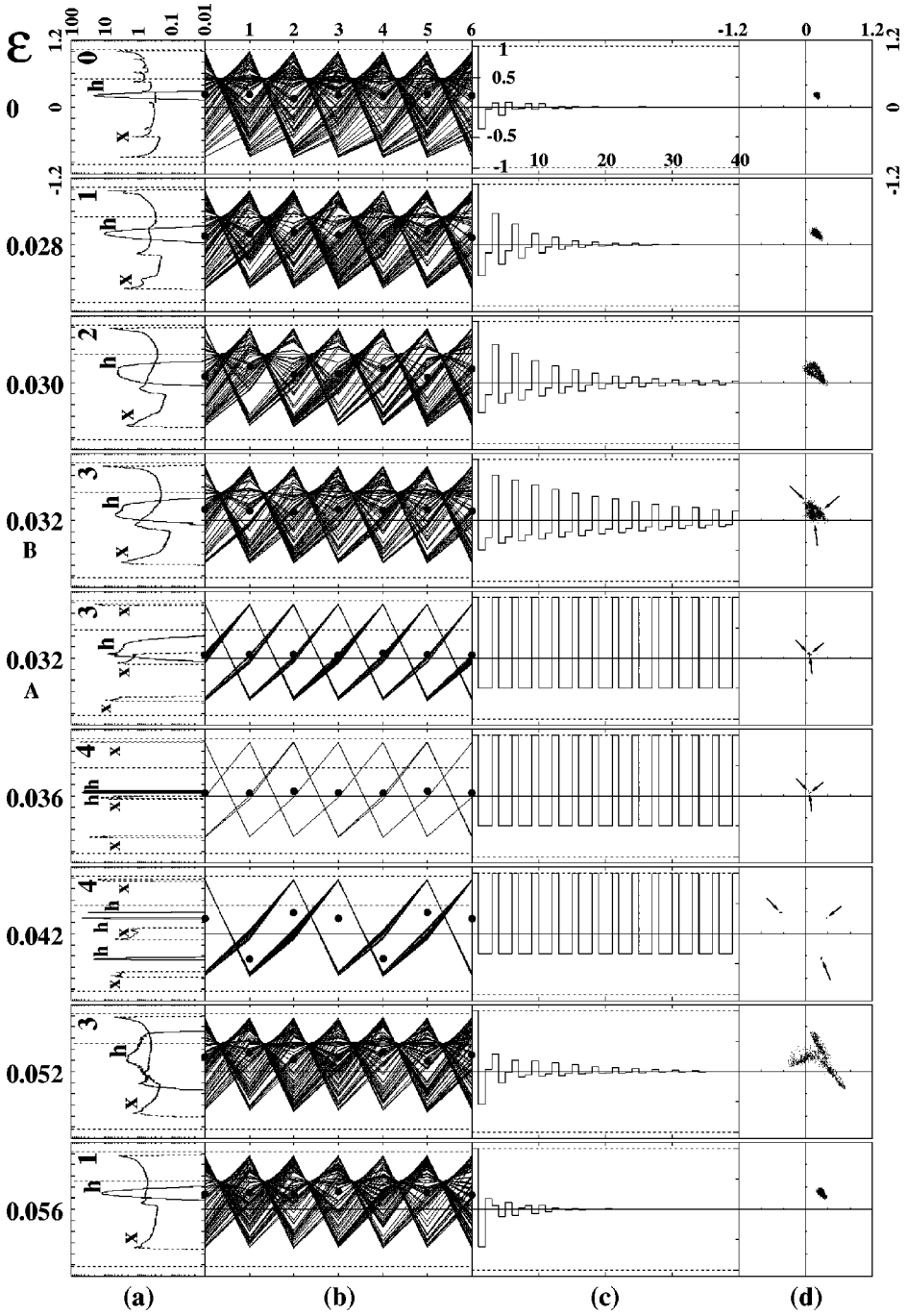

FIG. 4. The variation of the GCML dynamics with ε through the prominent MSD peak region. $N=10^3$ GCML with $a=1.90$, and the total iteration steps are 10^5 for each run. (a) The mean field distribution (marked as h), discarding the first 10^4 transient steps and the map distribution (x) averaged over the last 2×10^3 steps. (b) Clustering pattern. The lines are orbits of randomly selected 10^2 maps for the last seven steps, and the black circle is the mean field. (c) Temporal correlator between the two relative-coordinate vectors of the maps. Averaged over the last 10^3 steps. $\tau\approx 0$, 30, 70, 140, ∞, ∞, ∞, 50, and 0 for $\varepsilon=0,\ldots,0.056$. (d) The return maps for the same steps as (c). The arrows indicate the period three clusters.

4. Variation of dynamics with ε

Let us have a bird's eye view of Fig. 4. The row from $\varepsilon=0$ to 0.042 is the path from randomness to periodicity. At $\varepsilon=0$ the maps evolve freely in pure randomness. In this map distribution we observe many sharp peaks with a fractal structure. These reflect unstable fixed points of a single map. But the $h(n)$ distribution—the convolution of the map distribution—is Gaussian due to the CLT. It is sharp due to the LLN. The maps evolve randomly in a simple logistic pattern, and the correlator decays almost instantly. With increasing coupling ε, the coherence between maps is increased. The correlator reveals the precursor of the period-3 cluster attractor by its $p=3$ oscillation, and becomes prolonged. The map distribution turns into three broad bands losing subpeaks, and finally turns into sharp three δ peaks. Because of the increased coherence, the $h(n)$ distribution retains the orbital structure even after the convolution, and the rank of the $h(n)$ distribution is gradually increased. Finally the rank-4 distribution appears in the period-3 region.

In the period-3 region, we first observe the formation of the $p3c3$ MSCA, and at slightly higher ε the $p3c2$ cluster attractor. This region continues up to $\varepsilon\approx0.050$.

Beyond this, everything proceeds oppositely until $\varepsilon\approx0.058$. The rank gradually decreases and the correlator is shortened. Figure 4 ends at this position. At larger ε, the MSD shows small peaks and valleys in the range $\varepsilon\approx0.06$–0.1. Above $\varepsilon\approx0.10$ the correlator catches the precursor of the ordered two clustered regime. The path to periodicity is repeated, and eventually the period-2 regime starts around $\varepsilon\approx0.2$.

This is a bird's eye view of the turbulent regime at $a=1.90$ and $N=10^3$. For larger $N(\gtrsim 10^4)$, the MSD surface shows peaks and valleys more remarkably. The bulk of the above variation of the dynamics with ε also holds at the local scale, for each nearby pairing of a peak and valley. The peak $h(n)$ distribution is rank 3 and, with the change of ε to nearby valley values, the rank gradually decreases down to 1. At the higher (lower) nonlinearity a, we observe the same dynamics if the coupling is shifted to the larger (smaller) side with appropriate amount. For instance, the period-3 attractor region $\varepsilon \approx 0.032$–$0.050$ at $a=1.90$ is shifted to $\varepsilon \approx 0.06$–0.08 at $a=2.0$. This suggests curves of the balance in the a,ε parameter space. But why are the period 3 attractor states formed at this particular ε region? Are there no other cluster attractors with different periodicities? Our next task is to answer these questions, deriving the curves of the balance analytically.

IV. AN ANALYTIC APPROACH

A. Tuning condition and period-3 clusters

Let us consider an idealized (exact) MSCA. It is a state of a GCML under three conditions: (i) the N maps of the GCML split into c clusters with an exact population symmetry; (ii) the synchronization of maps is perfect, so that there is no variance of map positions in each of the clusters; and (iii) the clusters mutually oscillate around $p=c$ orbital points. Using this idealized state as a key, below we derive the tuning condition for the MSCA formation. For brevity we explain our approach with respect to the $p3c3$ MSCA in detail, but everything below also holds for the other MSCA's with higher periodicities. In a $p3c3$ MSCA three clusters A, B, C move cyclically round three fixed positions X_1, X_2, and X_3. Such a system of orbital points exists as a triple intersection point of three surfaces given by

$$\Sigma_i: \quad X_i = 1 - a\left[X_k^2 + \frac{\varepsilon}{3}(X_j^2 + X_k^2 - 2X_i^2)\right],$$
$$(i,j,k) \in \{(1,2,3),(2,3,1),(3,1,2)\}. \tag{4.1}$$

At $a=1.90$, and $\varepsilon=0.040$, for instance, we have two solutions $(0.96301,-0.00499,-0.72851)$ and $(0.95521, 0.07076,-0.69993)$; the former is stable, and the latter is unstable. In such an exact MSCA, the mean field $h(n)$ is a time-independent constant,

$$h(n) \equiv \frac{1}{N}\sum_{i=1}^{N} f(x_i(n)) = \frac{1}{3}\sum_{I=A,B,C} f(X_I(n)) = \frac{1}{3}\sum_{i=1}^{3} f(X_i)$$
$$= \frac{1}{3}\sum_{i=1}^{3} X_i \equiv h^*, \tag{4.2}$$

where $X_I(n)$ denotes the coordinate of the cluster I at time n, and the last equality follows from Eq. (2.2) or (4.1). Therefore, if a MSCA is produced, the GCML evolution equation (2.1) becomes

$$x_i(n+1) = (1-\varepsilon) f_a(x_i(n)) + \varepsilon h^* \quad (i=1,\ldots,N), \tag{4.3}$$

$$f_a(x) = 1 - ax^2,$$

where the time-dependent term $h(n)$ is replaced by a constant h^*. Every one of the maps evolves by a common equation at each step in Eq. (2.1), and further by a unique constant equation in Eq. (4.3). As noted by Perez and Cerdeira [17] some years ago, we can cast this unique equation into a standard logistic map with a reduced nonlinear parameter b,

$$y_i(n+1) = 1 - b(y_i(n))^2 \quad (i=1,\ldots,N). \tag{4.4}$$

by a linear scale transformation

$$y_i(n) = (1-\varepsilon+\varepsilon h^*)^{-1} x_i(n), \tag{4.5}$$

and the reduction rate of the nonlinearity parameter is given by

$$r \equiv \frac{b}{a} = (1-\varepsilon)(1-\varepsilon(1-h^*)). \tag{4.6}$$

At the MSCA, the mean field h^* is constant, so the reduction factor r is also constant. If the clusters of the MSCA oscillate in period 3, so do the maps $y_i(n)$—the two solutions $(x_1,x_2,x_3)^{(\nu)}$ $(\nu=1,2)$ of the cyclic equation (4.1) agree with the two sets of period-3 orbit points $(y(n),y(n+1),y(n+2))^{(\nu)}$ $(\nu=1,2)$ of the logistic map (4.4) modulo the scale factor in Eq. (4.5). The reduction factor r must reduce the high nonlinearity a of the GCML down to b in the period-3 window. It starts at $b_{\rm th} \equiv 7/4$ by the tangent bifurcation and, after sequential bifurcations and windows in the window, it closes at $b=1.79035$ by the crisis. The range of the period three window $b=1.75$–1.79035 requires a reduction factor r in the range 0.942–0.921 for $a=1.90$. Each r within this range gives a constraint curve[9] on ε,h^* plane via Eq. (4.6).

There is another constraint from self-consistency; the average value y^* of the transformed maps must also obey Eq. (4.5), so that

$$y^* \equiv \frac{1}{3}\sum_{i=1}^{3} y_i = (1-\varepsilon+\varepsilon h^*)^{-1} h^*. \tag{4.7}$$

Here y^* is a function of the nonlinear parameter b—it is simply an equal weight average of the period-3 stable orbits of the single logistic map [Eqs. (4.4)], and can be estimated solely by the property of the logistic map without any recourse to the GCML evolution equation. At a given y^* this again gives a constraint curve on the ε,h^* plane. Let us work out ε at the intersection of the two curves. By eliminating h^* from Eqs. (4.6) and (4.7), we obtain

$$\varepsilon = 1 - \frac{ry^*}{2} - \sqrt{r(1-y^*) + \left(\frac{ry^*}{2}\right)^2}, \tag{4.8}$$

and both $r=b/a$ and y^* on the right hand side are determined by b. This is the *tuning condition*. This predicts the

[9] It is possible to transform Eq. (2.1) formally to a standard form at each step, but then the reduction factor r may fluctuate step by step. Then it does not single out a line.

TABLE I. The $p=3$ periodicity manifestation in the turbulent regime. $a=1.90$, and $N=10^4$–10^6.

ε range	Prediction	MSD surface	State
0.032–0.0352[a]–0.037	0.0305–0.035192–0.0363	deep valley	bifurcated $p3c3$ MSCA
0.037–0.041	0.0363–0.0422	lower band	$p3c3$ MSCA
0.037–0.041		upper band	$p3c2$ cluster attractor
0.041–0.050	0.0422–0.0514	prominent peak	$p3c2$ cluster attractor

[a]The downwards cusp position of the MSD valley.

necessary value of the coupling ε for the GCML at a given a to form a MSCA due to the periodic attractor of the single logistic map with b. The function $y^*(b)$ is a well-known square well. $y^*\approx 0.284$ at $b=1.735$, slightly below the tangent bifurcation point $b_{\rm th}$, and it drops sharply ($y^*-y^*_{\rm th}\propto\sqrt{b_{th}-b}$) at $b_{\rm th}$. From a matching of the coefficients in $(f_b)^3(y)-y=b^6(f_b(y)-y)(\Pi_{i=1}^3(y-y_i))^2$, we obtain $y^*_{\rm th}=1/(3\times 2b)=2/21=0.095$. Similarly $y^*(b)=(1-\sqrt{4b-7})/6b$ up to the first bifurcation point $b=1.769$. Then $y^*(b)$ varies smoothly[10] around 0.08 until the end of the window ($b=1.7903$), and finally increases sharply ($y^*\approx 0.18$ at $b\approx 1.793$). This $y^*(b)$, put into Eq. (4.8), gives the following estimates of ε for $a=1.90$:

$$\begin{aligned} &A\text{:}\quad \varepsilon=0.0514 \quad \text{at}\ (b,y^*)=(1.735,0.284),\ r=0.913,\\ &B\text{:}\quad \varepsilon=0.0422 \quad \text{at}\ (b,y^*)=(1.750,0.095),\ r=0.921,\\ &C\text{:}\quad \varepsilon=0.0363 \quad \text{at}\ (b,y^*)=(1.769,0.069),\ r=0.931,\\ &D\text{:}\quad \varepsilon=0.0305 \quad \text{at}\ (b,y^*)=(1.790,0.080),\ r=0.942. \end{aligned} \tag{4.9}$$

Estimates *A*, *B*, *C*, and *D* are below the threshold, at the threshold, at the first bifurcation point in the window, and at the closing point of the window, respectively. Note that route $A\rightarrow D$ is in the direction of increasing b, which in turn is the direction of the decreasing coupling constant ε, since the larger b requires only a smaller nonlinearity reduction. We should stress that tuning condition (4.8) is a necessary condition. For the $p3c3$ MSCA to be stable, the orbit of the reduced logistic map must be also stable.[11] A period-3 logistic orbit still continues to exist even beyond the first bifurcation point *C*, but it is unstable. Therefore, for an exact $p3c3$ MSCA to be formed, the ε range must be within the estimates *C*-*B*, but neither within *D*-*C* nor beyond *D*. Similarly, an exact bifurcated $p3c3$ MSCA must be formed within *D*-*C*. Our tuning condition does not guarantee the formation of the MSCA but it does limit the ε range in which the formation is possible. The observed ranges of the $p3$ cluster attractors are listed in Table I. At $a=1.90$, a $p3c3$ MSCA is formed in the range $\varepsilon\approx 0.037$–0.041, and its bifurcated state in $\varepsilon\approx 0.032$–0.037. The predicted ranges are $\varepsilon=0.0363$–0.0422 and 0.0305–0.0363, respectively. In both cases, the agreement is remarkable, and we see that the formation actually occurs at any allowed ε value.

As for the $p3c2$ cluster state, we need caution in using the tuning condition. This condition is derived under the assumption of a constancy of the mean field. Thus, as a matter of principle, it cannot be applied for the asymmetrically populated state. However, the $p3c2$ state is formed with a slightly higher coupling ε, and the orbits of two clusters are approximately the same with the MSCA orbits. Therefore, the $p3c2$ cluster attractor is certainly still under the control of the period-3 window. We estimate the range by the extension of the period-3 window at the higher coupling side *B*-*A*—the intermittency region. This gives $\varepsilon=0.0422$–0.0514, in good agreement with the observed range of the $p3c2$ cluster attractor (≈ 0.041–0.050). It is interesting to note that the GCML final states at this ε range actually consist of two types depending on the initial condition; the $p3c2$ cluster attractor ($\approx 80\%$), as well as unstable period-3 clusters with mixing of maps (the rest). See Fig. 6 below. The estimate *B*-*A* intriguingly relates the intermittency of the element map to the GCML phase of coexistent stable and unstable periodic clusters. We are aware that we cannot take the success of the estimate for $p>c$ states on the same footing as that for the MSCA, but at least it gives a good rule of thumb for the $p>c$ state.

B. Foliation of the logistic windows in the turbulent regime

What is the case for other a values? Do the other windows also show up in the expected ε range in the turbulent regime? To check these questions systematically, let us note that the tuning condition defines a one-parameter (b) family of curves in the model parameter space (the a,ε plane) of the GCML. Each curve is labeled by b, and written as a function of the reduction factor r as

$$\begin{aligned} &(a^{(b)}(r),\varepsilon^{(b)}(r))\\ &\quad=\left(\frac{b}{r},1-\frac{ry^*(b)}{2}-\sqrt{r(1-y^*(b))+\left(\frac{ry^*(b)}{2}\right)^2}\right),\\ &\qquad r\leqslant 1. \end{aligned} \tag{4.10}$$

This emanates from the point $(a^{(b)},\varepsilon^{(b)})|_{r=1}=(b,0)$, and with the decrease of r it develops in the parameter space inthe direction in which both a and ε increase in a certain balance. If our success above is a general one, all GCML's with parameters set at $(a^{(b)}(r),\varepsilon^{(b)}(r))$ along a curve labeled

[10]The largest rapid variation is the tiny anti square well ($\Delta y^*\approx 0.01$) due to the 3×3 window at $b=1.7858$–1.7865.

[11]As we show in Sec. V, the Lyapunov exponents of the GCML at the $p3c3$ MSCA generally consist of an $(N-3)$-fold degenerate one and three nondegenerate ones. For the $p3c3$ MSCA to be stable, at least the former degenerate exponent must be negative, which implies that the reduced map orbit must be stable. That all these exponents are negative at the MSCA is also shown below.

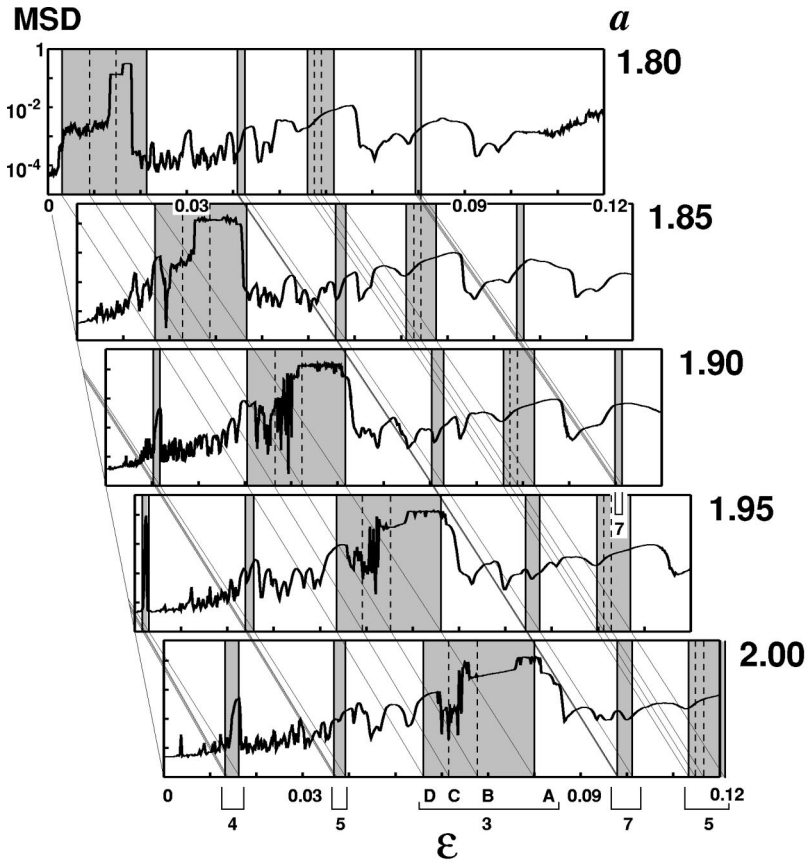

FIG. 5. The MSD of the mean field distribution plotted as a function ε for $N=10^4$ GCML in panels at $a=1.8$ (back), and $1.85,\ldots,2$ (front). $\varepsilon=0-0.12$ with inclement 10^{-4}. The foliation curves predicted for $p=4$, 5, 3, 7, and 5 windows flow underneath panels, and link the respective shaded foliation zones. For each zone there is a MSD valley at lower ε, and a peak at higher ε.

by b should be commonly controlled by the same dynamics of the single logistic map at b.

In Fig. 5 we find that this is indeed the case. Each panel shows the MSD of the $h(n)$ distribution as a function of ε at a given a as well as the expected zones for the manifestation of the outstanding six windows in Table II. Curves (4.10) are displayed underneath the panels, and link the respective zones. At each zone, a MSD valley due to the MSCA should appear in the lower ε side, and a MSD peak by $p>c$ cluster attractors at the nearby higher ε. We find that this works with almost no failure in all panels, and with respect to all six windows.

The effects of the logistic windows propagate along curves (4.10), which may be called *foliation curves*. The curve with the label b links together those GCML's commonly subject to the same logistic window dynamics at b. Accordingly the family of curves produces a *foliation* of the single map dynamics. The foliation occurs because, under the global interaction, the maps of the GCML form a macroscopically coherent state. Even though the coupling in the turbulent regime is very small, the coherence prevails over the GCML maps if the tuning condition is met. A few remarks are in order.

(1) Desynchronization along the foliation curve. The periodicity manifestation becomes weakened at a higher reduction, and there is a threshold $r_{\rm th}\approx 0.95$. For $r\approx 1$, both MSCA and associated $p>c$ clusters are formed in tight synchronization. Toward $r_{\rm th}\approx 0.95$, the clusters broaden. There is no mixing among the clusters as yet, but the maps move chaotically in each cluster. Below $r_{\rm th}$, we observe only the periodicity remnants—on the one hand the overlapping Gaussian $h(n)$ distribution along the curve which had the $p>c$ cluster above $r_{\rm th}$, and on the other hand the MSD-

TABLE II. The outstanding windows and their b, $y^*(b)$ values.

Period	A: intermittency[a]	B: lower threshold	C: the first bifurcation	D: closing point	Width[b]
7	1.5740, 0.3943	1.5748, 0.3857	1.5754, 0.3846	1.5762, 0.3847	0.0014
5	1.6220, 0.3610	1.6244, 0.3077	1.6284, 0.3012	1.6333, 0.3032	0.0089
7	1.6735, 0.3189	1.6740, 0.2676	1.6744, 0.2678	1.6749, 0.2677	0.0009
3	1.7350, 0.2836	1.7500, 0.0952	1.7685, 0.0685	1.7903, 0.0800	0.0403
5	1.8597, 0.1823	1.8606, 0.0984	1.8614, 0.0990	1.8623, 0.0987	0.0017
4	1.9390, 0.1287	1.9406, -0.1633	1.9415, -0.1668	1.9427, -0.1657	0.0021

[a]The starting point of intermittency.

[b]$\Delta b \equiv b_B - b_D$.

TABLE III. Samples of the sequences of attractors with $p \geqslant c$. $N=10^4$, and a in parentheses.

$p=4$: b:1.9406–1.9427[a]	($a=1.95$, $r\approx 0.995$)		
c	4 (MSCA)	3	2
ε	0.0019–0.0022	0.0022–0.0024	0.0024–0.0026
ε_{pred}[b]	0.0020–0.0022	0.0022––––	–––0.0030
$p=5$: b:1.6244–1.6333[a]	($a=1.66$, $r\approx 0.980$)		
c	5(MSCA)[c]	4	3
ε	0.00986–0.0118	0.0114–0.0124	0.0124–0.0130
ε_{pred}[d]	0.00950–0.0112	0.0112–––	–––0.0140

[a]The range of the window from B to D, i.e., the intermittent region is not included.
[b]The ε range predicted by the tuning condition and the window data in Table II. The predictions are from C-B for MSCA and B-A for $p>c$ states.
[c]For most events, the attractor is either bifurcated or consists of five bands.
[d]D-C for a MSCA and C-A for a $p>c$ cluster attractor, taking into account the bifurcation.

enhanced Gaussian (the hidden coherence) along that of MSCA. See Fig. 2.

(2) Left-right asymmetry of the MSD curves. The MSD curves in Fig. 5 (and 2) show an interesting feature—in each panel the smaller ε region (the left) has an ample amount of peaks and valleys, while the larger only a few broad ones. As for the single logistic map, on the other hand, there are as many windows in the smaller b as in the larger.

This is naturally understood by the difference in the reduction factor r between the zones in a panel. In a way, each panel is a screen which displays the windows of the single logistic map by using a macroscopic coherent state of the GCML. But the panels set at fixed a values are inclined—a smaller ε (the left) implies less reduction, i.e. $r\approx 1$. $r_{\rm th}$ divides the panel at $\varepsilon\approx 0.030$ via Eq. (4.8). The left sensitively displays the sharp peak-valley structure induced by cluster attractors. The right, on the other hand, can reflect only the accumulation of the periodicity remnants from nearby windows, being dominated by the prominent one at its respective zone. As a check we set the panels at fixed r values. Then they displayed windows without asymmetry, and with a higher sensitivity at r closer to one [18].

(3) Cluster attractors with higher periodicity. Let us search cluster attractors with a periodicity higher than 3. Here we give two samples in Table III.

$p=4$ *clusters*. These appear in the left most zone in the $a=1.95$ panel. From the window b data in Table II the necessary reduction from a is very small—$r\approx 0.995$—so we expect definite clusters. We indeed find the expected sequence of clusters[12] $p=4$, $c=4(\mathrm{MSCA})\rightarrow 3\rightarrow 2$, in tight synchronization at the right ε.

$p=5$ *clusters*. There are two $p=5$ windows in Table II. We choose the one at the lower b and set $b=1.66$, which amounts to $r=0.980$. Since r is in the midst of 1 and $r_{\rm th}$, we expect the clusters are not in complete synchronization, but yet there is no mixing of maps. Indeed the sequence of attractors $p=5$, $c=5(\mathrm{MSCA})\rightarrow 4\rightarrow 3$ is observed at the expected ε, and it terminates before the lowest one ($p5c2$).

V. STABILITY OF THE PERIOD THREE CLUSTERED MAP STATES

Here we adopt the Lyapunov analysis. As one superlative ability, it can be applied to both diverging and converging system orbits, so that it can detect the possible coexistence of multifold finial states depending on the initial configurations. We measure the maximum Lyapunov exponent $\lambda_{\max}$ by a standard method [19] which keeps track of an N-dimensional shift vector $\delta\mathbf{x}(n)$ evolving under the nonautonomous linearized equation associated with Eq. (2.1):

$$\delta x_i(n+1)=-2a\left\{\left(1-\varepsilon+\frac{\varepsilon}{N}\right)x_i(n)\,\delta x_i(n)+\frac{\varepsilon}{N}\sum_{j\neq i}x_j(n)\,\delta x_j(n)\right\}. \tag{5.1}$$

$\lambda_{\max}$ is the average of the logarithm of the expansion rate of the shift vector (with intermediate renormalizations). For both $\lambda_{\max}$ and the MSD, we discard the first transient 10^4 steps—generally it takes only 10^2–10^3 steps for the cluster formation.

Let us first check the ε dependence of the stability of attractors. We choose $N=10^6$, fix a at 1.90, and vary ε in the range 0.030–0.052 with the inclement $\Delta\varepsilon=10^{-4}$. In Fig. 6 we show $\lambda_{\max}$ in the upper part and the MSD in the lower part.[13]

In the $\lambda_{\max}$ plot we observe three remarkable structures of low $\lambda_{\max}$ events.

(i) *A seagull structure* ($\varepsilon=0.032$–0.037) with a sharp cusp at $\varepsilon=0.0352$—all events are bifurcated MSCA's with good population symmetry [$N_I/N\approx(1\pm 0.05)/6$]. Note that the events form also a seagull in the MSD, and the cusp

[12]The single cluster cannot be formed. The focusing by averaging does not act there, and the tiny variance is instantly amplified. It appears far in the coherent phase ($\varepsilon\gtrsim 0.4$ at $a=1.90$).

[13]For reference, the CPU time for the $N=10^6$ GCML is approximately 2 min for one measurement of $\lambda_{\max}$ (2^{12} steps for precision 10^{-4}) plus the MSD (10^4 steps) on a modest supercomputer VPP300/6. The total is 2 min$\times$40 (initial configurations) $\times$220 (ε values)$\approx$300 h.

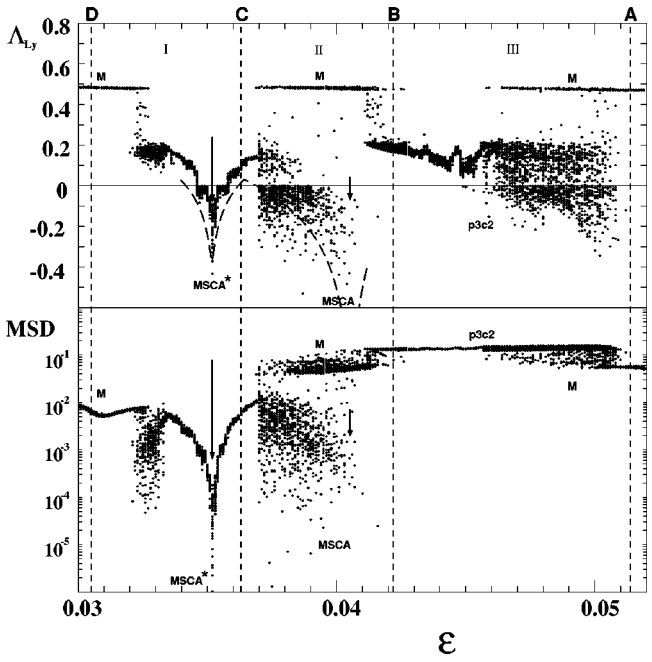

FIG. 6. The Lyapunov exponents (upper) and the MSD (lower) measured for 40 random initial configurations at each ε between 0.0300 and 0.0520 with inclement 10^{-4}. $a=1.90$ and $N=10^6$. The events in the seagull structures are in the bifurcated MSCA states, the first lower band events in the MSCA and the second ones the p3c2 attractor. These are formed in regions I (D-C), II (C-B) and III (B-A) separated by dashed lines, as expected. In bands M, the $p=3$ clusters are unstable, and the maps mix among them with $\tau \approx 100$. The dashed line shows the predicted $\lambda_{\max}$ for the exactly symmetric MSCA. Arrows show the predicted positions of the most linearly stable MSCA states.

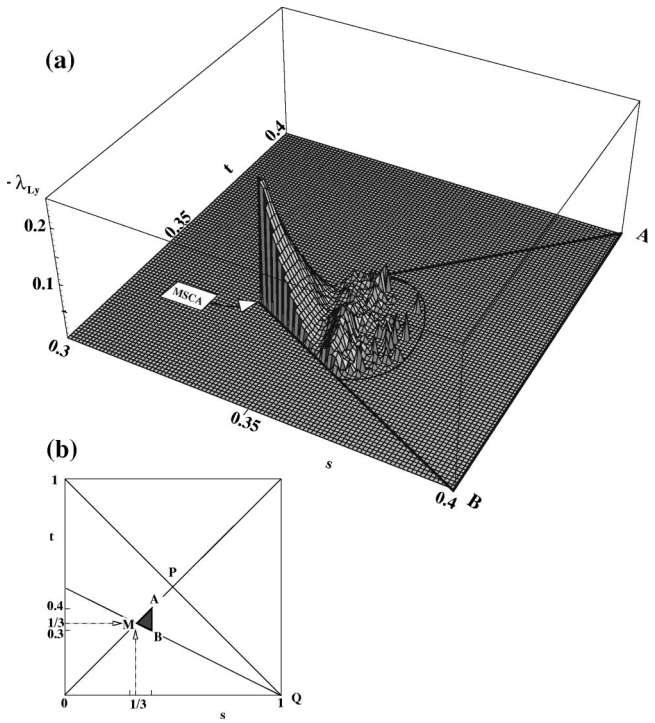

FIG. 7. (a) The maximum Lyapunov exponent of the bifurcated MSCA over the (s,t) plane. $\lambda_{\max}$ for events in one st bin are averaged, the sign is reversed ($-\lambda_{\max}$), and $\lambda_{\max}>0$ is truncated for a bird's eye view. $a=1.90$, $\varepsilon=0.035$, and $N=10^4$, and there are totally 2×10^4 events. (b) The triangle ΔPMQ is the allowed (s,t) region by the constraint $s \geqslant t$, $t \geqslant (1-s)/2$, $1 \geqslant s+t$. The bifurcated MSCA events accumulate in the top of the shaded tiny ΔAMB, which is again a tiny part of ΔPMQ.

positions agree precisely. *The bifurcated MSCA is more stable if the mean field fluctuation is lower, and it is most linearly stable* ($\lambda_{\max}=-0.38$) *with the minimum fluctuation* ($\delta h^2 \approx 2\times10^{-6}$).

(ii) *The first low band* ($\varepsilon=0.037$–0.041)—the $p3c3$ states. The population distributes around an exact MSCA—$\theta_I \equiv N_I/N \approx (1\pm0.15)/3$. The events near the lower boundary ($\lambda_{\max}<0$) are $p3c3$ events with good population symmetry and with a low MSD.

(iii) *The second low band* ($\varepsilon=0.041$–0.051)—the $p3c2$ cluster attractor. The corresponding MSD is, contrary to (ii), extremely high because of a lack of one cluster to minimize the $h(n)$ fluctuation (see Sec. III B 2).

The foliation of the critical points $A,\ldots,D$ from the period-3 window defines three ε regions I (D-C), II (C-B), III (B-A) [Eq. (4.9)]. Region I is the allowed region for the formation of the bifurcated MSCA (MSCA*), region II the p3c3 MSCA, and the $p3c2$ cluster attractor is expected in region III. As we see clearly in Fig. 6, regions I, II, and III embody structures (i), (ii), and (iii), respectively, in agreement with our prediction.

Let us note a remarkable feature in the events in the two wings of the seagull (i). Here all events come out with positive $\lambda_{\max}$ ($\approx$0.1–0.2). For a system with low degrees of freedom, the positive $\lambda_{\max}$ implies chaos. But here, even with positive $\lambda_{\max}$, the maps always form a bifurcated $p3c3$ state. There is actually no contradiction. The global motion of the clusters is periodic, but, inside each cluster, maps here evolve randomly with tiny amplitudes ($\lesssim 10^{-2}$) in sharp contrast against the complete synchronization at the cusp. The Lyapunov exponent measures the linear stability of the system with respect to the small deviation of the element position. It is sensitive to the microscopic motion of the element of the system, and hence yields the positive exponent. But for a larger deviation, nonlinear terms can become relevant and pull back the map.[14] This type of map motion—microscopically chaotic but macroscopically in the periodic clusters—may be called *confined chaos*. We hereafter devote ourselves into the investigation of two outstanding structures, namely the bifurcated MSCA seagull and the $p3c2$ cluster attractor.

The linear stability analysis of the bifurcated MSCA. In order to understand the salient cusp at $\varepsilon=0.0352$ in the Lyapunov exponent plot, let us consider the linear stability matrix of the GCML.

(1) For the configuration of maps in six clusters, the $N\times N$ linear stability matrix of the GCML for the evolution of one step can be written as

[14]We have verified this by inputting pulses on randomly selected maps. The analytic formulation of the nonlinear effect is most desired.

$$M_1=(1-\varepsilon)\begin{pmatrix} X_1E_1 & \cdots & 0 \\ 0 & \ddots & 0 \\ \cdots & \cdots & \cdots \\ 0 & \cdots & X_6E_6 \end{pmatrix} + \frac{\varepsilon}{N}\begin{pmatrix} X_1H_{11} & \cdots & X_6H_{16} \\ X_1H_{21} & \cdots & X_6H_{26} \\ \cdots & \cdots & \cdots \\ X_1H_{61} & \cdots & X_6H_{66} \end{pmatrix} \tag{5.2}$$

multiplied by an overall factor $-2a$, where $X_I(I=1,\ldots,6)$ are the coordinates of the clusters, E_I is an $N_I\times N_I$ unit matrix, and H_{IJ} is an $N_I\times N_J$ matrix with all elements 1. The N eigenvalues of M_1 consist of two sets. One is a set of six eigenvalues $\lambda^{(I)}=-2a(1-\varepsilon)X_I\,(I=1,\ldots,6)$, each (N_I-1)-fold degenerate. The degenerate eigenvectors of $\lambda^{(I)}$ are of the form Col.$(\mathbf{0};\ldots;\mathbf{0};(1,0,\ldots,0,-1,0,\ldots,0);\mathbf{0};\ldots;\mathbf{0})$, that is, all column blocks, each for one cluster, are fulfilled by $\mathbf{0}$ except for the Ith block which has 1 as the first element and -1 as one of the other N_I-1 elements. The eigenvector of $\lambda^{(I)}$ represents a shift of the system orbits within the Ith cluster. The other is a set of six (in general nondegenerate) eigenvalues λ_I, which are the same with the ones of the 6×6 stability matrix $M_{1;\mathrm{red}}$ associated with the cluster evolution

$$X_I(n+1)=(1-\varepsilon)f(X_I)+\varepsilon\sum_{J=1}^{6}\theta_J f(X_J),\quad (I=1,\ldots,6). \tag{5.3}$$

$M_{1;\mathrm{red}}$ for the cluster dynamics is derived from M_1 by $E_I\to 1$ and $H_{IJ}\to\theta_J$. The eigenvector of M_1 subject to λ_I is $(\xi_1^I\mathbf{1};\ldots;\xi_6^I\mathbf{1})$, with $(\xi_1^I,\ldots,\xi_6^I)$ being that of $M_{1;\mathrm{red}}$.

(2) The stability matrix M_p of the GCML for the evolution of p steps is given by the chain product of p of M_1 along the system orbit. The eigenvalues of M_p again consist of two sets. One is the set of six eigenvalues $\lambda^{(I)}=[-2a(1-\varepsilon)]^p\Pi_{k=1}^{p}X_I^k$, each (N_I-1)-fold degenerate, and the first set eigenvectors of M_1 remain the eigenvectors of this set. The other is the same with the ones of the $M_{p;\mathrm{red}}$—the pth iterate of $M_{1;\mathrm{red}}$. This mechanism holds at any population composition among the GCML clusters.

(3) Now, when the population symmetry among the clusters are exact, all of the maps obey a unique quadratic mapping [Eq. (4.3)] with a constant mean field h^* which is equivalent to a standard logistic map [Eq. (4.4)] with a reduced nonlinearity b via the scale transformation (4.5). For b from the first to the second bifurcation point in the $p=3$ window ($b_6=1.76852915$ to $b_{12}=1.777221618$), the reduced map y evolves in period 6, and so do the six GCML clusters. This is the bifurcated MSCA. We can write the correspondence as

$$\begin{array}{ccccccccc} y_0 & \to & y_1=f_b(y_0) & \to & \cdots & \to & y_5=(f_b)^5(y_0) & \to & y_0=(f_b)^6(y_0) \\ \begin{pmatrix} X_1 \\ X_2 \\ \vdots \\ X_6 \end{pmatrix} & \to & \begin{pmatrix} X_2 \\ X_3 \\ \vdots \\ X_1 \end{pmatrix} & \to & \cdots & \to & \begin{pmatrix} X_6 \\ X_1 \\ \vdots \\ X_5 \end{pmatrix} & \to & \begin{pmatrix} X_1 \\ X_2 \\ \vdots \\ X_6 \end{pmatrix}. \end{array} \tag{5.4}$$

In the MSCA, all six eigenvalues of M_6 in the first set degenerate into a single value $\Lambda\equiv[-2a(1-\varepsilon)]^6\Pi_{I=1}^{6}X_I$, with degeneracy $\Sigma_{I=1}^{6}(N_I-1)=N-6$. From Eqs. (5.4), (4.5), and (4.6) we find $\Lambda=(-2b)^6\Pi_{i=1}^{6}y_i$, that is, Λ is nothing but the Lyapunov eigenvalue of the single logistic map for the $p=6$ motion. As for the other set, the $M_{6;\mathrm{red}}$ for the symmetric configuration $\theta_I=1/6$ is a chain product of six matrices, that is, $M_{1;\mathrm{red}}^6M_{1;\mathrm{red}}^5\cdots M_{1;\mathrm{red}}^1$ with

$$M_{1;\mathrm{red}}^1=-2a\begin{pmatrix} (1-\varepsilon+\eta)X_1 & \eta X_2 & \cdots & \eta X_6 \\ \eta X_1 & (1-\varepsilon+\eta)X_2 & \cdots & \eta X_6 \\ \vdots & \cdots & \ddots & \vdots \\ \eta X_1 & \cdots & \cdots & (1-\varepsilon+\eta)X_6 \end{pmatrix},\quad \eta=\frac{\varepsilon}{6}, \tag{5.5}$$

and other five matrices are obtained by cyclically changing the orbit points X_I by Eq. (5.4). By a simple algebra using Eqs. (4.5) and (5.4), we find that the eigenvalues of M_6 in the second set, which are in turn the ones of $M_{6;\mathrm{red}}$, are Λ, with corrections of order η.

(4) Now we are ready to work out the seagull cusp position. Because Λ is proportional to the product of the period-6 orbital points of the single logistic map f_b, it becomes zero when one of the orbital points becomes zero. At this very instance, the $N-6$ Lyapunov exponents become $-\infty$ and the other six exponents also become very small in proportion to $\log(|\eta|)/6$. The b is a solution of $f_b^6(0)=0$ and the relevant solution $b_c=1.772892$ gives $\varepsilon_c=0.035192$ and $\lambda_{\max}=-0.361519$ for $a=1.90$—both are in remarkable agreement with the observed cusp of the GCML Lyapunov exponent.

Over the seagull ε range, $M_{6;\mathrm{red}}$ has four complex $[(\lambda_k,\lambda_k^*),\ k=1,2)]$ and two real eigenvalues and gives four exponents. $\lambda_{\max}$ is given by one of the two sets of complex eigenvalues, while the $(N-6)$-fold degenerate exponent

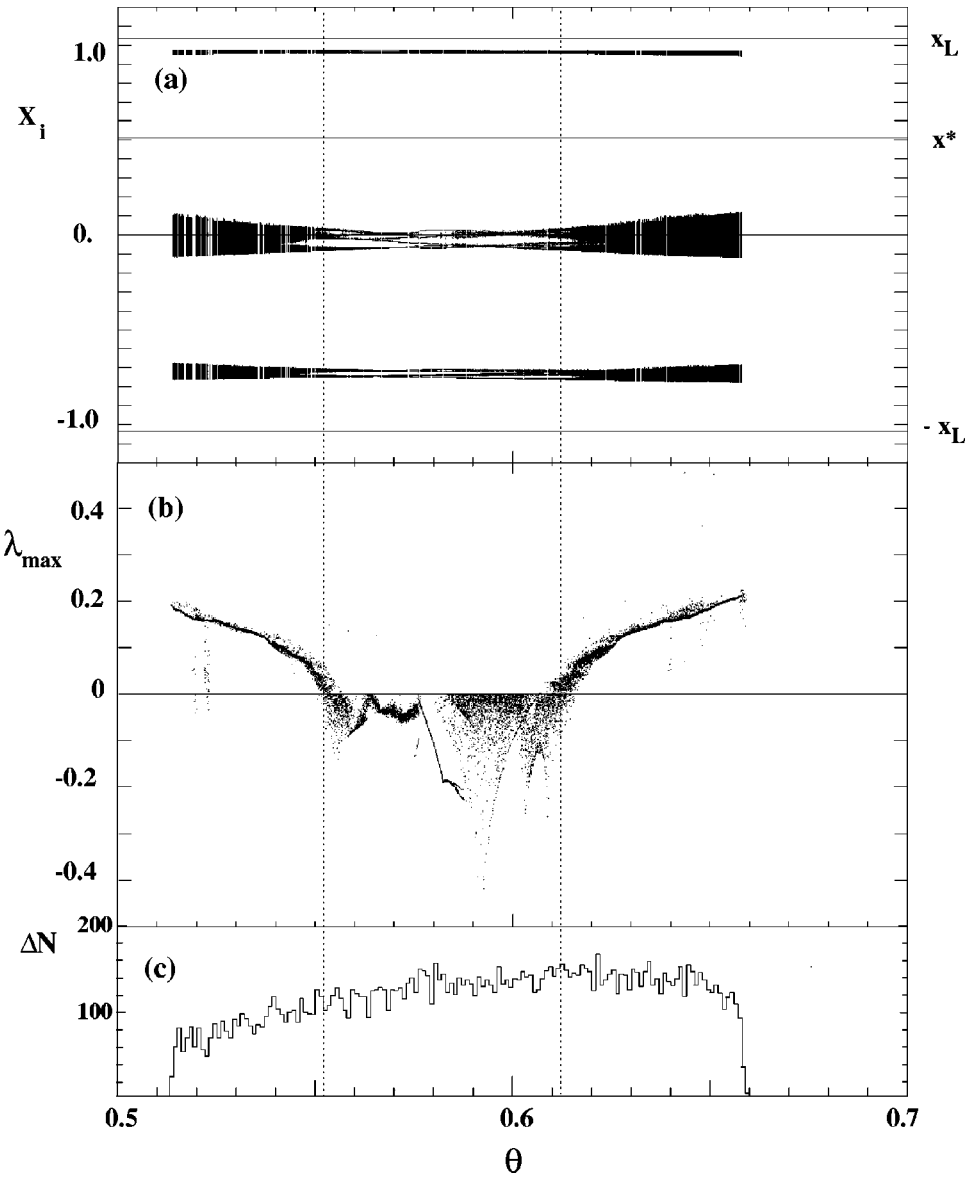

FIG. 8. (a) The orbits of a $p3c2$ cluster attractor for the last 512 steps. (b) The maximum Lyapunov exponents. (c) The number of events in each bin ($\Delta\theta = 10^{-3}$) plotted at a population ratio θ for 18 341 events (83%), with stable cluster formation among totally 22 000 events. $N = 10^4$, $a = 1.90$, and $\varepsilon = 0.048$. Dotted lines are used to draw the eye, and to separate tightly bound cluster states (central) and the confined chaos (two edges).

from Λ runs in the midst of the four. The predicted $\lambda_{\max}$ is shown in Fig. 6, and explains the data well. The slight deviation off the cusp is due the small population unbalance; it is the larger of the larger MSD events.

The dependence of the λ_{max} on the population ratios. We proceed with the following algorithm after detecting the clusters by the gaps. The six MSCA* clusters evolve in the bifurcated orbits of a $p3c3$ MSCA. They can be regarded as three doublets—(C_{I_1}, C_{I_2}), $I = 1$, 2, and 3, so that the two clusters C_{I_1} and C_{I_2} in a doublet evolve close together. We combine the two populations in a doublet into one and define s, t and u as $(N_{I_1} + N_{I_2})/N$ in decreasing order.

In Fig. 7(a), we exhibit the averaged $-\lambda_{\max}$ on the (s,t) plane from the 2×10^4 random events for $N = 10^4$ GCML with $a = 1.90$, $\varepsilon = 0.035$. At the top of the pyramid-shaped surface $\lambda_{\max}$ is negative, and at a minimum. It occurs precisely at the most symmetric population configuration. We also find that the bulk of the events are formed with almost perfect population symmetry. They accumulate in the top of a tiny triangle ΔAMB ($s, t \leqslant 0.4$) which is again a tiny part of the kinematically allowed region ΔPMQ. $\lambda_{\max}$ is negative over the bulk of events around the symmetric point—the MSCA is linearly stable. The exception occurs only near the boundary (the round curve), where $\lambda_{\max}$ is mostly positive and small ($\lambda_{\max} \lesssim 0.05$), and the maps form the confined chaos.

The $p3c2$ cluster attractor. We have performed a similar high statistics analysis at $a = 1.90$ and $\varepsilon = 0.048$ for the same $N = 10^4$ GCML. The final states are twofold: a $p3c2$ cluster attractor (83%) and unstable $p3$ clusters with mixing (the rest). Hereafter we analyze the former in Fig. 8. In the region $0.55 \leqslant \theta \leqslant 0.61$, the $p3c2$ clusters are tightly bounded and linearly stable. Here the dynamics of the GCML is reduced to that of two clusters. Just like the $p2c2$ state in the two ordered clustered phases [1], the $p3c2$ orbits bifurcate with the change of θ—the ratio θ can be used as a control parameter even in the turbulent regime.

However, there is a remarkable difference as well. In $p2c2$ there is no stable attractor for θ outside the window. In the turbulent regime, on the other hand, a loosely bound $p3c2$ state can be formed—the three orbital bands in the edge regions. This state is again confined chaos. $\lambda_{\max}$ is posi-

tive ($0 \leqslant \lambda_{max} \leqslant 0.2$), and the maps fluctuate randomly in each of the two clusters. But the clusters are in a macroscopic period-3 motion. As the probability distribution shows, this is formed as frequently as the $p3c2$ cluster attractor. The state of confined chaos at the unbalanced population is a characteristic feature of the cluster attractors in the turbulent regime.

VI. CONCLUSION

In this paper we have revisited the GCML of the logistic maps, and studied in detail its so-called turbulent regime. We have presented our new phenomenological findings in an extensive statistical analysis, which as a whole reveal that the turbulent regime is under the systematic control of the periodic windows of the element logistic map. In particular we have shown that the hidden coherence occurs only in a very limited regions in the turbulent regime. Some observations were partially reported in earlier articles by one of us (T.S.) [21], which include the finding of the manifestation of $p3c3$ MSCA and $p3c2$ attractor state.

There appears remarkable $p3c3$ MSCA states as well as $p3c2$ cluster attractors induced by the period-3 window of the element map. Our tuning condition predicts by a family of curves how the dynamics of the element map foliates in the parameter space of the GCML. This successfully explains the salient peak-valley structures of the MSD surface, and tells us where to see the remarkable sequence of the cluster attractors of the type $p,c=p \rightarrow (p-1) \rightarrow (p-2) \rightarrow \cdots$.

We have also investigated the linear stability of the period-3 cluster attractors. Both the $p3c3$ MSCA and its bifurcated state are linearly stable when the population symmetry is good, and the MSD of the mean field is minimized. We have analytically explained the value of the coupling ε at a given a for the formation of the most stable bifurcated MSCA. The $p3c2$ cluster attractor is also linearly stable in the θ window even though the MSD of the $h(n)$ is quite high. For the unbalanced population configuration the system forms an interesting state of confined chaos, which is a characteristic feature of the cluster attractors in the turbulent regime.

There remain interesting unsolved problems. One concerns the state of confined chaos newly found in the turbulent regime. This is a state consisting of a few clusters in macroscopic periodic motion and maps move around chaotically inside each clusters. Regarding the linear stability, the Lyapunov exponent is positive. It is tempting to single out the nonlinear effect which confines the maps in periodic clusters. A related problem is the onset of incomplete synchronization with the decrease of the reduction factor r along the foliation curves. The other problem is concerned with the variation of the dynamics with the system size N. We have found that the system becomes an extremely sensitive mirror of the element dynamics with increasing N. The salient evidence is shown in Figs. 2 and 3, but we are unable to explain why this is so. In field theory the vacuum at the spontaneous breakdown of the symmetry is stable only when the degree of dynamical degree of freedom is infinite [20]. If we may regard the randomness of GCML maps as a symmetry, the MSCA with no $h(n)$ fluctuation corresponds to a vacuum at the symmetry breakdown, and the formation of it by synchronization corresponds to the onset of an ordered parameter. The resolution of the finite size effect in the GCML is tempting, since it may bridge the synchronization of the maps and the onset of the order parameter in the field theory in quantitative terms. As a whole this work is an exploration of order in chaos, and we have found that the turbulent regime of the GCML is controlled by the foliation of the single logistic dynamics.

Note added. Recently, we have noted related works on the foliation of the logistic windows. A. P. Parravano and M. G. Cosenza independently reported the MSCA [22]. T. Shibata and K. Kaneko also independently found the foliation of windows in the mean field fluctuations, and called it a ''tongue structure'' [23]. Both parallel works [22,23] overlap ours with respect to foliation, but neither the manifestation of type $p>c$ attractors nor the stability of the MSCA were discussed there.

ACKNOWLEDGMENTS

It is our pleasure to thank Hayato Fujigaki, Fumio Masuda, Ko-ichi Nakamura, Maki Tachikawa, Norisuke Sakai, Wolfgang Ochs, and Hidehiko Shimada for useful discussions and encouragement. This work was supported by the Faculty Collaborative Research Grant from Meiji University, Grant-in-Aids for Scientific Research from Ministry of Education, Science and Culture of Japan, and Grant for High Techniques Research from both organizations.

[1] K. Kaneko, Phys. Rev. Lett. **63**, 219 (1989).
[2] K. Kaneko, Phys. Rev. Lett. **65**, 1391 (1990).
[3] A. S. Pikovsky and J. Kurths, Phys. Rev. Lett. **72**, 1644 (1994).
[4] K. Kaneko, Physica D **55**, 368 (1992); **86**, 158 (1995).
[5] K. Kaneko, Physica D **34**, 1 (1989); J. P. Crutchfield and K. Kaneko, in *Directions in Chaos*, edited by B.-L. Hao (World Scientific, Singapore, 1987).
[6] K. Kaneko, Physica D **41**, 137 (1990).
[7] K. Kaneko, Physica D **54**, 5 (1991); S. Sinha, D. Biswas, M. Azam, and S. V. Lawande, Phys. Rev. A **46**, 3193 (1992).
[8] L. M. Pecora and T. L. Carroll, Phys. Rev. Lett. **64**, 821 (1990); T. L. Carroll and L. M. Pecora, Physica **67**, 126 (1993).
[9] J. M. Kowalski and G. L. Albert, Phys. Rev. A **42**, 6260 (1990).
[10] A. Maritan and J. R. Banavar, Phys. Rev. Lett. **72**, 1451 (1994).
[11] H. Fujigaki, M. Nishi, and T. Shimada, Phys. Rev. E **53**, 3192 (1996); H. Fujigaki and T. Shimada, *ibid.* **55**, 2426 (1997).
[12] A. S. Pikovsky, M. G. Rosenblum, and J. Kurths, Europhys. Lett. **34**, 165 (1996); M. G. Rosenblum, A. S. Pikovsky, and J. Kurths, Phys. Rev. Lett. **76**, 1804 (1996).
[13] J. J. Hopfield, Proc. Natl. Acad. Sci. USA **79**, 2554 (1982); W.

A. Little, Math. Biosci. **19**, 101 (1974); D. J. Amit, H. Gutfreund, and H. Sompolinski, Phys. Rev. A **32**, 1007 (1985).
[14] *Spin Glass Theory and Beyond*, edited by M. Mézard, G. Parisi, and M. A. Virasoro (World Scientific, Singapore, 1987).
[15] A. Lasota and M. C. Mackey, *Chaos, Fractals, and Noise* (Springer, New York, 1994), Chaps. 3. 2 and 7. 4; Y. Oono and Y. Takahashi, Prog. Theor. Phys. **63**, 1804 (1980); W. Just, J. Stat. Phys. **79**, 429 (1995).
[16] S. V. Ershov and A. B. Potapov, Physica D **86**, 523 (1995).
[17] G. Perez and H. A. Cerdeira, Phys. Rev. A **46**, 7492 (1992).
[18] T. Shimada and K. Kikuchi (unpublished).
[19] I. Shimada and T. Nagashima, Prog. Theor. Phys. **61**, 1605 (1979); G. Benettin, L. Galgani, A. Giorgilli, and J. M. Strelcyn, C.R. Seances Acad. Sci., Ser. A **14**, A-431 (1978).
[20] See, e.g. S. Weinberg, *The Quantum Theory of Fields* (Cambridge University Press, Cambridge, 1996), Vol. 2. A macroscopic broken rotational symmetry state realized by a chair is discussed on p. 195.
[21] T. Shimada, Technical Report of IEICE, NLP97-159, 71 (1998); and an early version of this paper, Mem. Inst. Sci. Tech. Meiji Univ. **37**, 1 (1998); preprint, chao-dyn/9810007.
[22] A. P. Parravano and M. G. Cosenza, Int. J. Bifuration Chaos **9**, 2331 (1991).
[23] T. Shibata and K. Kaneko, Physica D **124**, 177 (1998).